Ligand Environment of the S-2 State of Photosystem II: A Study of the Hyperfine Interactions of the Tetranuclear Manganese Cluster by 2D N-14 HYSCORE Spectroscopy

6 AUTHORS, INCLUDING:

Sergey Milikisiyants
Rensselaer Polytechnic Institute

12 PUBLICATIONS **81** CITATIONS

SEE PROFILE

Ruchira Chatterjee
Lawrence Berkeley National Laboratory

24 PUBLICATIONS **159** CITATIONS

SEE PROFILE

Amanda Weyers
Rensselaer Polytechnic Institute

12 PUBLICATIONS **229** CITATIONS

SEE PROFILE

K. V. Lakshmi
Rensselaer Polytechnic Institute

78 PUBLICATIONS **2,408** CITATIONS

SEE PROFILE

Ligand Environment of the S₂ State of Photosystem II: A Study of the Hyperfine Interactions of the Tetranuclear Manganese Cluster by 2D ¹⁴N HYSCORE Spectroscopy

Sergey Milikisiyants, Ruchira Chatterjee, Amanda Weyers, Ashley Meenaghan, Christopher Coates, and K. V. Lakshmi*

Department of Chemistry and Chemical Biology and The Baruch '60 Center for Biochemical Solar Energy Research, Rensselaer Polytechnic Institute, Troy, New York 12180

Received: July 3, 2010

The solar water-splitting protein complex, photosystem II, catalyzes the light-driven oxidation of water to dioxygen in Nature. The four-electron oxidation reaction of water occurs at the tetranuclear manganese−calcium−oxo catalytic cluster that is present in the oxygen-evolving complex of photosystem II. The mechanism of light-driven water oxidation has been a subject of intense interest, and the oxygen-evolving complex of photosystem II has been studied extensively by structural and biochemical methods. While the recent X-ray crystal structures and single-crystal EXAFS investigations provide a model for the geometry of the tetranuclear manganese−calcium−oxo catalytic cluster, there is limited knowledge of the protein environment that surrounds the catalytic cluster. In this study, we demonstrate the application of two-dimensional hyperfine sublevel correlation spectroscopy to determine the magnetic couplings of the catalytic cluster with the ¹⁴N atoms of surrounding amino acid residues in the S₂ state of the oxygen-evolving complex of photosystem II. We utilize two-dimensional difference spectroscopy to facilitate unambiguous assignments of the spectral features and identify at least three separate ¹⁴N atoms that are interacting with the catalytic cluster in the S₂ state. The results presented here, for the first time, identify previously unknown ligands to the catalytic cluster of photosystem II and provide avenues for the assignment of residues by site-directed mutagenesis and the refinement of computational and mechanistic models of photosystem II.

Introduction

The solar water-splitting protein complex, photosystem II (PSII), catalyzes the light-driven oxidation of water to dioxygen in Nature. The four-electron oxidation reaction of water occurs at the tetranuclear manganese−calcium−oxo (Mn_4Ca−oxo) catalytic cluster that is present in the oxygen-evolving complex (OEC) of PSII.[1−5] The mechanism of light-driven water oxidation has been a subject of intense interest,[6] and the OEC of PSII has been studied extensively by structural, spectroscopic, biochemical, and computational methods.[1−4,7−18] The recent 2.9−3.8 Å resolution X-ray crystal structures[1−4,19] and single-crystal EXAFS studies[18] provide a model for the geometry of the Mn_4Ca−oxo catalytic cluster. These findings are in agreement with the magnetic couplings determined by EPR spectroscopy.[20,21]

It is suggested that the binding and activation of the substrate water molecules at the Mn_4Ca−oxo cluster in the OEC of PSII are facilitated by key amino acid residues that are ligated to the catalytic cluster. Despite extensive investigations there is limited knowledge and consensus on the protein environment that surrounds the Mn_4Ca−oxo catalytic cluster of PSII.[14] Previous electron nuclear double resonance (ENDOR) and one-dimensional (1D) multifrequency electron spin-echo envelope modulation (ESEEM) spectroscopy studies have yielded contradictory structural information on the ligand environment of the Mn_4Ca−oxo cluster in the S₂ state of the OEC of PSII.[22,23] The continuous-wave (cw) ¹⁵N ENDOR spectroscopy investigations have suggested the presence of hyperfine interactions with two ¹⁵N nuclei either from a single histidine ligand or possibly from two separate ligands to the Mn_4Ca−oxo cluster in the S₂

state.[22] In contrast, the multifrequency ¹⁴N ESEEM study by Britt and co-workers has identified a single ¹⁴N nucleus that interacts strongly with the Mn_4Ca−oxo cluster and this nitrogen was assigned to a proximal histidine residue.[23] In ENDOR and 1D ESEEM spectroscopy, it is often difficult to resolve electron−nuclear couplings from more than one nucleus due to the overlap of spectral features. This experimental limitation could possibly account for the different interpretations that were derived in the previous studies.

We report here a pulsed two-dimensional (2D) hyperfine sublevel correlation (HYSCORE) spectroscopy study to probe the electron−nuclear hyperfine interactions of the S₂ state of the OEC of PSII. We use 2D ¹⁴N HYSCORE spectroscopy to measure the hyperfine couplings of the Mn_4Ca−oxo cluster (effective $S = 1/2$ electron spin) with the nitrogen-14 (¹⁴N) nuclei ($I = 1$ nuclear spin) of the surrounding amino acid ligand environment. There are several advantages that render 2D HYSCORE spectroscopy a powerful tool to probe the OEC of PSII. First, addition of the second dimension in 2D ¹⁴N HYSCORE spectroscopy dramatically improves the spectral resolution as compared to one-dimensional (1D) 2-pulse and 3-pulse ESEEM and ENDOR spectroscopy techniques.[24] In comparison to 1D ESEEM spectroscopy, the electron−nuclear hyperfine couplings in 2D ¹⁴N HYSCORE spectroscopy are detected on a much larger frequency space, which provides enhanced resolution. Second, in the case of the $S = 1/2$ electron spin (as well as an effective $S = 1/2$ center, such as, the S₂ state of PSII), the nuclear frequencies are correlated in two dimensions, which crucially simplifies analysis of hyperfine interactions and allows for unambiguous interpretation of the experimental spectra. In this study, we use the power of 2D

* To whom correspondence should be addressed. Phone: (518) 276 3271. Fax: (518) 276 4887. E-mail: lakshk@rpi.edu.
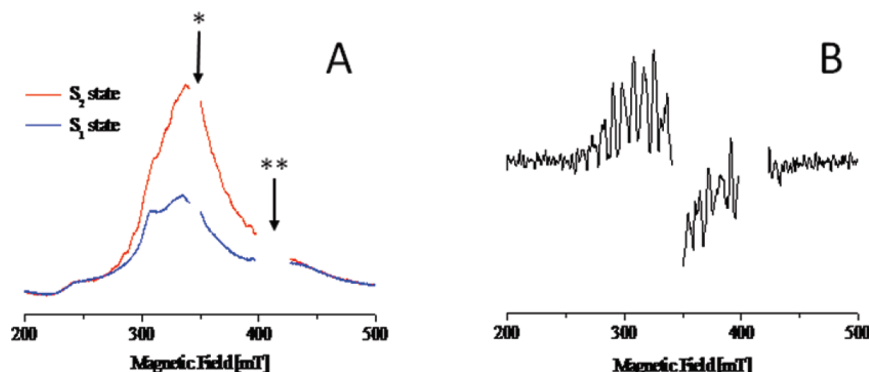
Figure 1. (A) Echo-detected EPR spectrum of intact PSII with OEC trapped in the S_2 (red line) and S_1 (blue line) state. (B) Numerical derivative of the S_2-minus-S_1 difference EPR spectrum that is obtained from the data shown in A. (*) is the region of the spectrum containing the EPR signal from the $Y_D^\bullet$ radical; (**) is the region of the spectrum containing unavoidable resonator artifacts.

[14]N HYSCORE difference spectroscopy to identify at least three separate ^{14}N nuclei that are interacting with the Mn$_4$Ca−oxo cluster in the S_2 state of the OEC of PSII. The results presented here directly address the lack of experimental data on the ligand environment of the Mn$_4$Ca−oxo cluster of PSII and identify previously unknown ligands to the cluster.

Materials and Methods

Preparation of Photosystem II Complexes and Trapping of the S State Intermediates. The PsbB hexa-histidine-tagged (His-tagged) mutant *Synechocystis* PCC 6803 cells were grown at 24 °C in BG-11 medium.[25] The PSII complexes were isolated from the cells by minor modifications of previously published procedures.[26] The PSII samples were monitored by SDS-polyacrylamide gel electrophoresis, and the densitometry scans showed very minor PSI contamination (<3%). The O_2-evolution rates were monitored by a Clark electrode and were typically 4800 μmol of O_2 (mg of Chl)$^{-1}$ h^{-1}.[27] The PSII complexes used for the EPR measurements of the S_2 and S_1 states of the OEC were resuspended in buffer containing 50 mM 2-(N-morpholino)ethanesulfonic acid-sodium hydroxide (MES-NaOH), 20 mM calcium chloride (CaCl$_2$), 5 mM magnesium chloride (MgCl$_2$), 0.03% (w/v) dodecyl-β-D-maltoside (β-DM), and 30% glycerol (w/v) at pH 6.0. The PSII samples were preincubated with 200 μM potassium ferricyanide prior to illumination. The S_2 state was cryo-trapped by 45 s illumination at 200 K followed by rapid freezing (5−10 s) at 77 K, in the dark. The S_1 state was accumulated by dark adapting the PSII sample at 0 °C for 30 min.

Pulsed EPR Spectroscopy. EPR spectra were recorded on a custom-built continuous-wave (cw)/pulsed X-band Bruker Elexsys 580 spectrometer. The pulsed EPR measurements were conducted with a dielectric flex-line probe ER 4118-MD5 (Bruker BioSpin Corp., Billerica, MA) and a dynamic continuous-flow cryostat CF935 (Oxford Instruments, Oxfordshire, U.K.). The operating microwave frequency was set to 9.71 GHz to best match the broad band of the strongly overcoupled pulsed resonator. All of the pulsed EPR spectra were acquired at 5 K.

For the echo-detected field sweep spectra, the primary electron spin echo was generated using the pulse sequence ($\pi/2-\tau-\pi$ echo). The echo was integrated over a 40 ns time window, which was centered at the maximum of the echo signal. The length of the $\pi/2$ and π pulse was 12 and 24 ns, respectively. The interpulse separation, τ, was 144 ns, and the delay in the pulse sequence is defined as the difference in the starting point of the pulses. The spectra were recorded over the range of 300 mT centered at 350 mT.

For the 2D HYSCORE spectra, the echo amplitude was measured using the pulse sequence ($\pi/2-\tau-\pi/2-t_1-\pi-t_2-\pi/2$ echo) with an 8 and 16 ns length for the $\pi/2$ and π pulse, respectively, and an 8 ns detector gate (that is centered at the maximum of the echo signal). The delays in the pulse sequence are defined as the difference in the starting point of the pulses. The echo intensity was measured as a function of t_1 and t_2, where t_1 and t_2 were incremented in steps of 16 ns from an initial value of 40 and 32 ns, respectively. There were 256 steps used for each dimension. The 8 ns time difference between the initial value of t_1 and t_2 was set to take into account the difference in length between the $\pi/2$ and π pulse. This provided symmetric spectra in both dimensions. The unwanted echoes and antiechoes were eliminated by applying a 16-step phase-cycling procedure. A third-order polynomial baseline was subtracted from the resulting time-domain spectra. The corrected spectra were zero filled to obtain a [2048 × 2048] matrix and Fourier transformed using a fast Fourier transformation (FFT) algorithm. The frequency domain spectra were plotted as the amplitude (absolute value) of the 2D frequency components.

Results and Discussion

In the echo-detected EPR spectra shown in Figure 1A and 1B, we observe the characteristic 'multiline' EPR spectrum of the S_2 state ($S = 1/2$) (shown as a red trace) and the dark stable background EPR spectrum of the S_1 state (shown as a blue trace) of PSII.[7,28−30] Upon comparison of the line shape of the EPR spectra of the S_2 and S_1 state, we observe that in addition to the multiline EPR signal that arises from the [55]Mn electron−nuclear hyperfine interactions of the Mn$_4$Ca−oxo cluster in the S_2 state there are at least two additional paramagnetic centers that contribute to the observed spectrum: (i) a very narrow signal at $g \approx 2$ from the redox-active tyrosyl radical, $Y_D^\bullet$ (this signal is marked by an asterisk (*) in Figure 1A), and (ii) the heme Fe(III) center of cytochrome b_{559} (Cyt b_{559}) that displays a rhombic spectrum due to the presence of g anisotropy ($g_X = 1.5$, $g_Y = 2.3$, and $g_Z = 3.0$).[31] In the present study, we use S_2-minus-S_1 state difference spectroscopy to eliminate the dark-stable spectral contribution from the heme Fe(III) center of Cyt b_{559}. The derivative of the S_2-minus-S_1 state EPR difference spectrum is shown in Figure 1B.

On the basis of the S_2-minus-S_1 EPR difference spectrum in Figure 1B, we perform 2D ^{14}N HYSCORE spectroscopy at three different magnetic field positions (B) of 355 ($g' = 1.95$), 380 ($g' = 1.82$), and 337.5 mT ($g' = 2.055$), respectively, where the effective g value (g') is calculated as $g' = h\nu_{mw}/\beta_e B$ using the microwave frequency (ν_{mw}) and Bohr magneton (β_e). We
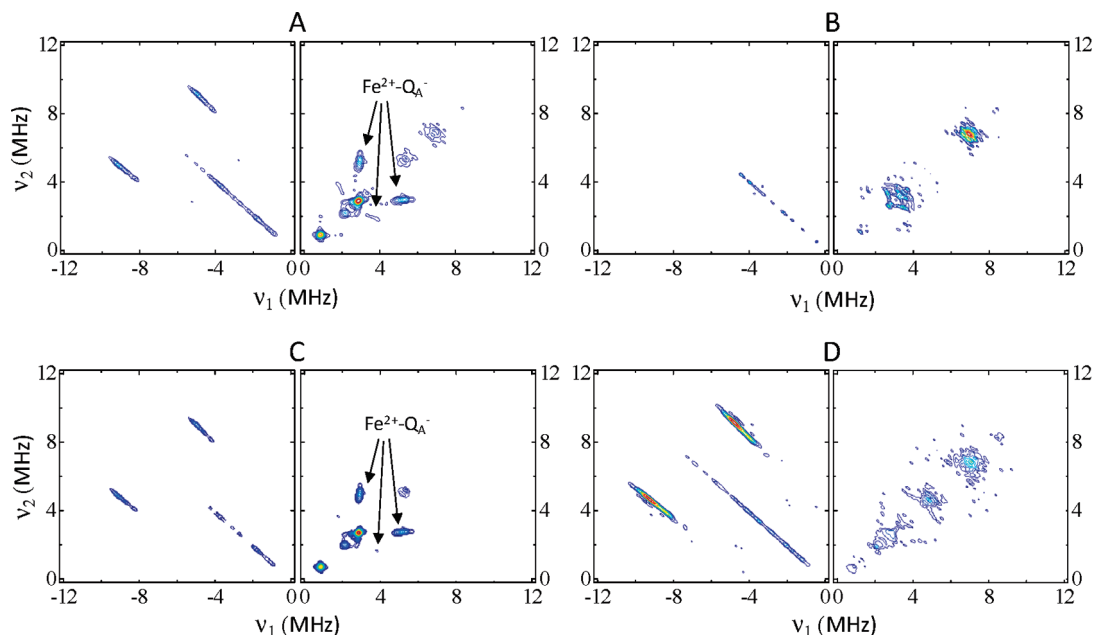
Figure 2. $(-,+)$ and $(+,+)$ quadrants of the 2D ^{14}N HYSCORE spectrum of intact PSII with the OEC in (A) the S$_2$ state at $g = 1.95$ with $\tau = 132$ ns and (B) the S$_1$ state at $g = 1.95$ with $\tau = 132$ ns, (C) the difference between the spectra shown in A and B, and (D) the S$_2$ state at $g = 1.82$ with $\tau = 140$ ns.

also incorporate three different values for the interpulse delay, τ, of 132, 140, and 176 ns in the 2D ^{14}N HYSCORE measurements. We select the magnetic field position(s) for the acquisition of the 2D ^{14}N HYSCORE spectrum to preclude overlap with the residual signal from the dark-stable Y$_D^{\bullet}$ radical of PSII, and we optimize the interpulse delay(s) in the pulse sequence to avoid blind spots in the spectrum.

Figure 2A and 2B displays the 2D ^{14}N HYSCORE spectra of the S$_2$ and S$_1$ state of PSII, respectively, acquired at the magnetic field position of $g' = 1.95$. On the basis of the EPR spectra shown in Figure 1A, we expect that the 2D ^{14}N HYSCORE spectrum of the S$_2$ state at the magnetic field position of $g' = 1.95$ (Figure 2A) could exhibit hyperfine couplings due to the Mn$_4$Ca–oxo cluster in the S$_2$ state and the heme Fe(III) center of Cyt b_{559}. To identify the spectral contributions from the heme Fe(III) center of Cyt b_{559}, we examine the 2D ^{14}N HYSCORE spectrum of intact PSII with the OEC in the dark-stable S$_1$ state (Figure 2B). As can be seen in Figure 2B, there is a small spectral contribution from the heme Fe(III) center of Cyt b_{559} in the S$_1$ state of the OEC of PSII. Therefore, we isolate the spectral features that arise from the S$_2$ state of PSII with the observation of the S$_2$-minus-S$_1$ 2D ^{14}N HYSCORE difference spectrum (Figure 2C).

In the S$_2$-minus-S$_1$ 2D ^{14}N HYSCORE difference spectrum in Figure 2C, we observe the ^{14}N hyperfine couplings of the Mn$_4$Ca–oxo cluster in the S$_2$ state of the OEC of PSII. In addition, we also observe weak ^{14}N hyperfine couplings that could be due to the Q$_A^-$ center in the S$_2$ state of PSII. When the S$_1$ state is illuminated at cryogenic temperature (200 K), it undergoes a one-electron oxidation and advances to the S$_2$ state. The electron is transferred to the primary quinone, Q$_A$, which is reduced to the semiquinone anion, Q$_A^-$ (also referred to as the 'iron-Q$_A^-$ couple' as the Q$_A^-$ semiquinone is magnetically coupled to the nonheme Fe(II) center of PSII).[5] Thus, in addition to the presence of ^{14}N hyperfine couplings from the S$_2$ state, there exists the possibility of ^{14}N hyperfine contributions from Q$_A^-$ (or iron–Q$_A^-$ couple) in the S$_2$-minus-S$_1$ 2D ^{14}N HY-SCORE difference spectrum. The spectral features that we tentatively assign to Q$_A^-$ (labeled as Fe^{2+}–Q$_A^-$ in Figure 2C)

are similar to previously published hyperfine couplings of the Q$_A^-$ center of PSII.[32,33]

We also acquire the 2D ^{14}N HYSCORE spectrum of the S$_2$ and S$_1$ state of PSII at the magnetic field position of $g' = 1.82$ and 2.055. We observe that the unwanted spectral features from weakly coupled ^{14}N nuclei from Q$_A^-$ are absent at the magnetic field position of $g' = 1.82$ (Figure 2D) and 2.055 (Figure 3). Further, comparison of the EPR signals at the magnetic field positions of $g' = 1.82$ and 2.055 indicates that the spectral intensity of the S$_2$ 'multiline' EPR signal at the magnetic field position of $g' = 2.055$ is significantly higher than the spectral intensity at the magnetic field position of $g' = 1.82$. This indicates that data acquisition at the magnetic field position of $g' = 2.055$ would allow for a better signal-to-noise ratio. Thus, we use $g' = 2.055$ for acquisition of the 2D ^{14}N HYSCORE spectrum to determine the electron–nuclear couplings of the Mn$_4$Ca–oxo cluster in the S$_2$ state of the OEC of PSII.

Shown in Figure 3A–D are the 2D ^{14}N HYSCORE spectra that are acquired at the magnetic field position of $g' = 2.055$ with an interpulse delay of $\tau = 140$ (Figure 3A and 3B) and 176 ns (Figure 3C and 3D). For both values of the interpulse delay, the spectrum of the dark-stable S$_1$ state (Figure 3B and 3D) displays ^{14}N hyperfine cross peaks from the heme Fe(III) center of Cyt b_{559}.[31] We find that in the case of $\tau = 140$ ns, the relative intensity of the spectral features due to Cyt b_{559} are significantly suppressed with respect to those of the S$_2$ state (Figure 3A and 3C). Hence, the final 2D ^{14}N HYSCORE spectra of the S$_2$ state of the OEC of PSII described below are acquired at the magnetic field position of $g' = 2.055$ with an interpulse delay of $\tau = 140$ ns.

Figure 4A and 4B displays the $(-,+)$ and the $(+,+)$ quadrant, respectively, of the S$_2$-minus-S$_1$ 2D ^{14}N HYSCORE difference spectrum that is acquired at a magnetic field position of $B = 337.5$ mT ($g' = 2.055$) with $\tau = 140$ ns. As can be seen in Figure 4A, we observe four cross peaks (or ridges) in the $(-,+)$ quadrant of the 2D ^{14}N HYSCORE difference spectrum. These ridges are identified as the double-quantum (DQ) and single-quantum (SQ) correlations of a ^{14}N nucleus (N^I) that is strongly hyperfine coupled ($A > 2\nu_I$) to the Mn$_4$Ca–oxo cluster in the
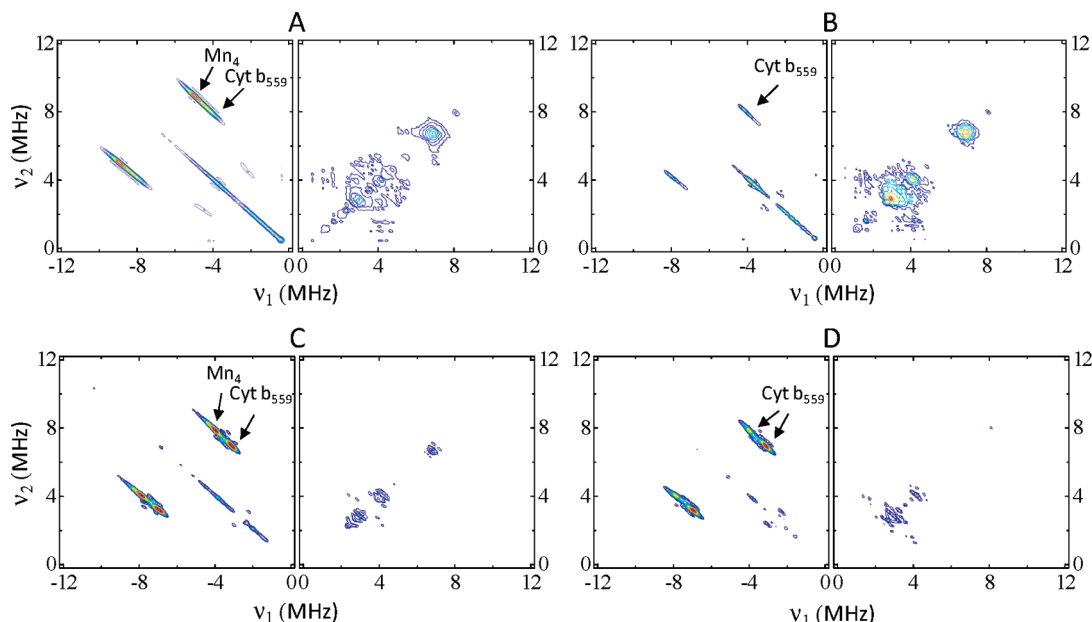
Figure 3. $(-,+)$ and $(+,+)$ quadrants of the 2D ^{14}N HYSCORE spectrum of intact PSII with the OEC in (A) the S_2 state at $g = 2.055$ with $\tau = 140$ ns, (B) the S_1 state at $g = 2.055$ with $\tau = 140$ ns, (C) the S_2 state at $g = 2.055$ with $\tau = 176$ ns, and (D) the S_1 state at $g = 2.055$ with $\tau = 176$ ns.
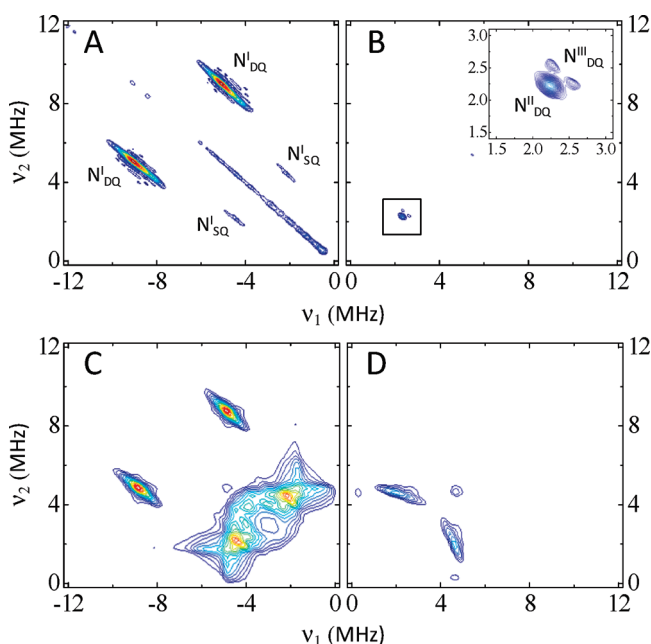

Figure 4. 2D contour plot of the (A) $(-,+)$ quadrant and (B) $(+,+)$ quadrant of the 2D ^{14}N HYSCORE spectrum, obtained as the difference between the spectrum of PSII with the OEC trapped in the S_2 and S_1 state, (C) the $(-,+)$ quadrant and (D) the $(+,+)$ quadrant of the simulated 2D ^{14}N HYSCORE spectrum for the ^{14}N nucleus, N^I, which is strongly interacting with the $Mn_4Ca-oxo$ cluster in the S_2 state of the OEC of PSII.

S_2 state of the OEC of PSII.[34−36] The separation between the ridges within each pair of cross peaks (that are symmetric with respect to the antidiagonal) is close to quadruple and double of the corresponding ^{14}N Zeeman frequency ($\nu_I^N = 1.0384$ MHz). Further, the separation between the cross peaks within the couple increases proportionally with the increase of the magnetic field (compare Figures 2D and 3A). This indicates that the ^{14}N Zeeman interaction is the origin of the separation between the cross peaks.

In contrast, we detect three closely located cross peaks in the $(+,+)$ quadrant of the 2D ^{14}N HYSCORE difference

spectrum of the S_2 state of the OEC of PSII (Figure 4B). The first cross peak that is well pronounced is located on the diagonal at a frequency $\sim$2.25 MHz, which is close to twice the ^{14}N Zeeman frequency ($2\nu_I^N = 2.077$ MHz). This cross peak is assigned to the double-quantum transition of at least one weakly hyperfine coupled ($A < 2\nu_I$) ^{14}N nucleus (N^{II}) in the vicinity of the $Mn_4Ca-oxo$ cluster in the S_2 state of the OEC of PSII. The small shift from the position corresponding to twice the ^{14}N Zeeman frequency is caused by the quadrupolar interaction of the N^{II} nucleus. The absence of any resolved structure outside of the diagonal indicates a weak hyperfine interaction of the N^{II} nucleus with the effective $S = 1/2$ electron spin of the $Mn_4Ca-oxo$ cluster in the S_2 state.

In addition, there are two cross peaks which are weaker in intensity that are symmetric with respect to the diagonal, and these are assigned to the double-quantum transitions of a weakly coupled ^{14}N nucleus (N^{III}). Once again, as mentioned above the small shift along the diagonal from twice the ^{14}N Zeeman frequency is due to the quadrupolar interaction of the N^{III} nucleus. The separation of the cross peaks along the antidiagonal is due to the hyperfine interaction of the nucleus with the unpaired electron spin of the $Mn_4Ca-oxo$ cluster in the S_2 state.

We note that in a 2D HYSCORE experiment, the presence of possible pulse imperfections could result in the appearance of unwanted peaks along the diagonal. In this study, the use of S_2-minus-S_1 state difference spectroscopy eliminates possible artifacts except for those that could arise from the three-pulse ESEEM contribution due to incomplete excitation by the third microwave pulse of the 2D HYSCORE pulse sequence. We have performed additional 2D HYSCORE measurements in the absence of the third pulse. The results of these experiments unambiguously confirm that the cross peaks that are observed in the $(+,+)$ quadrant arise from the N^{II} and N^{III} nuclei.

The knowledge of the hyperfine parameters is essential for the assignment of the nuclei that are magnetically coupled to a paramagnetic center. The observation of well-pronounced DQ and SQ ridges for the N^I nuclei permits determination of principal components of both the hyperfine and the quadrupole tensors. The correlation frequencies for a double-quantum (DQ)

TABLE 1: Hyperfine and Quadrupolar Interaction Parameters of the ^{14}N Nuclei Obtained by Spectral Simulation of the S$_2$-Minus-S$_1$ 2D HYSCORE Spectrum of the S$_2$ State of PSII That Is Shown in Figure 4A and 4B

nitrogen type	$|A_1|$ [MHz]^a	$|A_2|$ [MHz]^a	$|A_3|$ [MHz]^a	$K^2(3 + \eta^2)$ [MHz^2]	$e^2qQ/\hbar$ [MHz]	η
I	5.34 ± 0.2	6.7 ± 0.5	8.0 ± 0.2	0.705 ± 0.1	$1.56{-}1.95$	$0.6{-}1$
II	<0.3	<0.3	<0.3	0.22 ± 0.06	$0.8{-}1.2$	$0{-}1$
III^b	0.04 ± 0.05	$0.04{-}0.28 \pm 0.05$	0.28 ± 0.05	0.35 ± 0.03	$1.13{-}1.43$	$0{-}1$

^{a} The hyperfine components follow the convention $|A_1| \leq |A_2| \leq |A_3|$. ^{b} The values for $|A_1|$ and $|A_3|$ are the lower and upper limits of the hyperfine tensor components, respectively.

transition in the case of $S = 1/2$ and $I = 1$ spins are given by following expressions[34]

$$v_\alpha = \\ \pm 2\sqrt{(v_I + A_1/2)^2 l_1^2 + (v_I + A_2/2)^2 l_2^2 + (v_I + A_3/2)^2 l_3^2 + K^2(3 + \eta^2)} \quad (1)$$

$$v_\beta = \\ \pm 2\sqrt{(v_I - A_1/2)^2 l_1^2 + (v_I - A_2/2)^2 l_2^2 + (v_I - A_3/2)^2 l_3^2 + K^2(3 + \eta^2)} \quad (2)$$

where v_I is the Zeeman frequency for the given magnetic field ($v_I^N = 1.0384$ MHz for $B = 337.5$ mT), $A_{1,2,3}$ are the principal components of the hyperfine tensor, $l_{1,2,3}$ are the direction cosines of the magnetic field, $K = e^2qQ/4\hbar$, Q is the quadrupole moment interacting with the electric field gradient q, and η is the asymmetry parameter. The signs of eqs 1 and 2 are equal for the case of weakly interacting nuclei and the cross peak appears in the $(+,+)$ and $(-,-)$ quadrants of the 2D HYSCORE spectrum. In the case of strongly interacting nuclei, the signs of v_α and v_β are opposite and the cross peak appears in the $(-,+)$ and $(+,-)$ quadrants.

Since in powder samples all of the orientations are excited by the microwave pulses at X-band EPR frequency, the cross peaks form extended ridges on the 2D frequency domain. The ridges are confined between two points which are determined by the orientation of the magnetic field along the canonical directions corresponding to the smallest (A_1) and to the largest (A_3) hyperfine components. The coordinates of these two points for the upper ridge are easily obtained from the eqs 1 and 2

$$\left[v_\alpha^1 = \pm 2\sqrt{(v_I + A_1/2)^2 + K^2(3 + \eta^2)}; \right. \\ \left. v_\beta^1 = \pm 2\sqrt{(v_I - A_1/2)^2 + K^2(3 + \eta^2)} \right] \quad (3)$$

$$\left[v_\alpha^2 = \pm 2\sqrt{(v_I + A_3/2)^2 + K^2(3 + \eta^2)}; \right. \\ \left. v_\beta^2 = \pm 2\sqrt{(v_I - A_3/2)^2 + K^2(3 + \eta^2)} \right] \quad (4)$$

For the lower ridge, the order of the coordinates for each point is reversed, i.e., $[v_\alpha;v_\beta]$ point of the upper ridge corresponds to the $[v_\beta;v_\alpha]$ point of the lower ridge.

In the present study, for the strongly interacting ^{14}N nucleus, N^I, the coordinates of two extreme positions of the upper DQ ridge, [-6.17 MHz; 10.22 MHz] and [-3.65 MHz; 7.60 MHz], provide an accurate determination of the components of the hyperfine tensor, $A_1 = 5.34$ MHz, $A_3 = 8.0$ MHz, and the value of $K^2(3 + \eta^2) = 0.705$ MHz^2. To obtain the values for A_2 and η we perform numerical simulations using the '*saffron*' function of the EasySpin (version 3.1.0) software.[37] For the spectral simulations, A_1, A_3, and $K^2(3 + \eta^2)$ are fixed at the values

determined above. As an approximation, we assume that the principal axis frames of the hyperfine and quadrupole tensors are collinear. The best fit of the experimental and simulated spectra is obtained with $A_2 = 6.7$ MHz and $\eta = 0.9$ (the simulations of the $(+,-)$ and $(+,+)$ quadrants of the 2D ^{14}N HYSCORE spectrum are shown in Figure 4C and 4D). However, a range of values $A_2 = 6.2{-}7.2$ MHz and $\eta = 0.6 - 1$ are in agreement with the simulations of the experimental 2D ^{14}N HYSCORE spectra. Please note that the simulations of the $(+,-)$ and $(+,+)$ quadrants of the 2D ^{14}N HYSCORE spectrum that are shown in Figure 4C and 4D contain additional features that are not observed in the experimental 2D ^{14}N HYSCORE spectra in Figure 4A and 4B. This is because the additional peaks that are observed in the simulated spectrum are an order of magnitude weaker in intensity and are comparable to the overall noise level of the experiment. Hence, the weak features that are present in the simulation are not observed in the experimental spectrum.

For the second ^{14}N nucleus, N^{II}, one DQ cross peak is observed corresponding to the correlation frequencies $v_\alpha \approx v_\beta \approx 2\sqrt{(v_I^2 + K^2(3 + \eta^2))} = 2.25$ MHz, providing the value of $K^2(3 + \eta^2) = 0.22$ MHz^2. The homogeneous width of this cross peak is determined by the decay time of the corresponding modulations in the time domain spectra. The width of the cross peak also increases along the antidiagonal direction due to the hyperfine interaction. Since it is difficult to separate the two contributions, we provide a conservative estimate of the upper limit for the hyperfine components $|A_{1,2,3}| \leq 0.3$ MHz for the ^{14}N nucleus, N^{II} that is interacting with the Mn$_4$Ca$-$oxo cluster in the S$_2$ state of the OEC of PSII.

For the third ^{14}N nucleus, N^{III}, the position of the upper DQ ridge is limited by the extreme positions with coordinates [2.63 MHz; 2.16 MHz] and [2.43 MHz; 2.36 MHz]. Application of eqs 3 and 4 to these coordinates yield the following values: $A_1 = 0.04$ MHz, $A_3 = 0.28$ MHz, and $K^2(3 + \eta^2) = 0.35$ MHz^2. The inverse of the time interval along each dimension of the HYSCORE experiment is comparable to the difference of the estimated hyperfine components, A_1 and A_3. Thus, the value that is obtained for A_1 and A_3 in this study represents the upper and lower limit, respectively, of the hyperfine components. The hyperfine and quadrupolar interaction parameters are summarized in Table 1.

The hyperfine and quadrupole parameters of the strongly interacting nitrogen nucleus, N^I, that are obtained in the present study (Table 1) are in excellent agreement with previous 1D ESEEM experiments at a series of microwave frequencies ranging from 9.5 to 30.8 GHz.[23] The results indicate that a histidine residue, most likely the imino nitrogen atom, is coordinated to the Mn(III) ion of the Mn$_4$Ca$-$oxo cluster in the S$_2$ state of the OEC of PSII. It is known that the quadrupole coupling constant, $e^2qQ/4\hbar$ is 3.3 ± 0.3 MHz for both uncoordinated peptide ^{14}N atoms and the imino ^{14}N atom of the histidine (imidazole side chain).[38] However, on coordination with a transition-metal ion, the value of the quadrupole coupling

constant is reduced to ~2 MHz for an imino nitrogen atom of the histidine[39] while it slightly increases for a peptide nitrogen atom.[40] The quadrupole constant for the ^{14}N nucleus, N^I, that is observed in this study is too small to be attributed to a peptide nitrogen atom. However, it is excellent agreement with the range of values that have been reported for the imino nitrogen atom of a histidine interacting with a metal cluster.[39] Thus, we assign the hyperfine-coupled N^I nucleus as an imino nitrogen atom of a histidine residue that is coordinated to the $Mn_4Ca-oxo$ cluster in the S_2 state of the OEC of PSII. This assignment is in agreement with previous suggestions that a histidine residue is directly coordinated to the $Mn_4Ca-oxo$ cluster in the OEC.[41]

The hyperfine tensor of the ^{14}N nucleus, N^I, that is observed in this study is not in agreement with previous cw ^{15}N ENDOR spectroscopy studies that indicated that the $Mn_4Ca-oxo$ cluster interacts with two nitrogen nuclei with hyperfine coupling constants of 3.7 and 0.7 MHz.[22] Taking into account the difference of the gyromagnetic ratio of the ^{15}N and ^{14}N isotopes, the larger hyperfine coupling constant of 3.7 MHz obtained in the cw ENDOR study would correspond to a hyperfine coupling constant of 2.64 MHz in this study. This value is much less than any of the three principal hyperfine components that are obtained for the ^{14}N nucleus, N^I (Table 1).

By exploiting the power of the higher resolution of 2D HYSCORE spectroscopy, for the first time, we demonstrate the presence of two additional ^{14}N nuclei, N^{II} and N^{III}, that are weakly hyperfine coupled to the $Mn_4Ca-oxo$ cluster in the S_2 state of the OEC of PSII. These interactions have previously been elusive using 1D ESEEM and ENDOR spectroscopy techniques. The value for the quadrupolar interaction of N^{II} is too small to be attributed to either an imino or an amino nitrogen atom of a histidine residue[39] or a peptide nitrogen atom.[42] The quadrupolar interaction of the N^{II} nucleus is in agreement with that previously reported for the terminal nitrogen atom of amino acids.[38] Although the X-ray crystal structures and the computational models of photosystem II suggest the presence of nitrogen atoms in the vicinity of the $Mn_4Ca-oxo$ cluster,[1–4,16,17,43–46] these structures do not display a terminal nitrogen atom of an amino acid side chain as a potential ligand to the cluster. This could be due to the limited resolution of currently available X-ray crystal structures of photosystem II. Thus, at the present time the unambiguous assignment of the N^{II} nitrogen remains a topic for further investigations.

The value of the quadrupolar interaction of the N^{III} nucleus can most reliably be attributed to the presence of the amino nitrogen atom that likely belongs to the same histidine residue as the directly coordinated imino nitrogen (N^I) that is discussed above. Previous studies of transition-metal–imidazole complexes have demonstrated that the hyperfine constant of the distal nitrogen atom is typically more than an order of magnitude less than that of the directly coordinated proximal nitrogen atom of the imidazole group.[47] The value that is obtained for the hyperfine components of both the N^{III} and the N^I nitrogen atoms correspond to this finding and provide additional support for the presence of a histidine ligand that is coordinated to the $Mn_4Ca-oxo$ cluster in the S_2 state of the OEC of PSII. The results presented here, for the first time, identify three ^{14}N atoms that are magnetically coupled to the catalytic cluster of photosystem II and provide a template for the nitrogen ligation of the $Mn_4Ca-oxo$ cluster in the S_2 state of the OEC of PSII. This study presents opportunities for the assignment of residues by site-directed mutagenesis and for the refinement of computational and mechanistic models of PSII.

Note Added after ASAP Publication. This paper was published on the Web on August 3, 2010. Two reference citations were misnumbered in the Results and Discussion section. The corrected version was reposted on August 19, 2010.

References and Notes

(1) Zouni, A.; Witt, H. T.; Kern, J.; Fromme, P.; Krauss, N.; Saenger, W.; Orth, P. *Nature* **2001**, *409*, 739.

(2) Kamiya, N.; Shen, J. R. *Proc. Natl. Acad. Sci. U.S.A.* **2003**, *100*, 98.

(3) Ferreira, K. N.; Iverson, T. M.; Maghlaoui, K.; Barber, J.; Iwata, S. *Science* **2004**, *303*, 1831.

(4) Loll, B.; Kern, J.; Saenger, W.; Zouni, A.; Biesiadka, J. *Nature* **2005**, *438*, 1040.

(5) Debus, R. J. *Biochim. Biophys. Acta* **1992**, *1102*, 269.

(6) McEvoy, J. P.; Brudvig, G. W. *Phys. Chem. Chem. Phys.* **2004**, *6*, 4754.

(7) Brudvig, G. W.; Thorp, H. H.; Pecoraro, V. L. *Adv. Chem. Ser.* **1995**, *246*, 249.

(8) Peloquin, J. M.; Britt, R. D. *Biochim. Biophys. Acta, Bioenerg.* **2001**, *1503*, 96.

(9) Messinger, J.; Nugent, J. H. A.; Evans, M. C. W. *Biochemistry* **1997**, *36*, 11055.

(10) Ahrling, K. A.; Peterson, S.; Styring, S. *Biochemistry* **1998**, *37*, 8115.

(11) Kulik, L. V.; Epel, B.; Lubitz, W.; Messinger, J. *J. Am. Chem. Soc.* **2005**, *127*, 2392.

(12) Yachandra, V. K.; Sauer, K.; Klein, M. P. *Chem. Rev.* **1996**, *96*, 2927.

(13) Chu, H. A.; Hillier, W.; Law, N. A.; Babcock, G. T. *Biochim. Biophys. Acta, Bioenerg.* **2001**, *1503*, 69.

(14) Debus, R. J. *Coord. Chem. Rev.* **2008**, *252*, 244.

(15) Yano, J.; Pushkar, Y.; Glatzel, P.; Lewis, A.; Sauer, K.; Messinger, J.; Bergmann, U.; Yachandra, V. *J. Am. Chem. Soc.* **2005**, *127*, 14974.

(16) Sproviero, E. M.; Gascon, J. A.; McEvoy, J. P.; Brudvig, G. W.; Batista, V. S. *Curr. Opin. Struct. Biol.* **2007**, *17*, 173.

(17) Sproviero, E. M.; Gascon, J. A.; McEvoy, J. P.; Brudvig, G. W.; Batista, V. S. *Coord. Chem. Rev.* **2008**, *252*, 395.

(18) Yano, J.; Kern, J.; Sauer, K.; Latimer, M. J.; Pushkar, Y.; Biesiadka, J.; Loll, B.; Saenger, W.; Messinger, J.; Zouni, A.; Yachandra, V. K. *Science* **2006**, *314*, 821.

(19) Guskov, A.; Kern, J.; Gabdulkhakov, A.; Broser, M.; Zouni, A.; Saenger, W. *Nat. Struct. Mol. Biol.* **2009**, *16*, 334.

(20) Peloquin, J. M.; Campbell, K. A.; Randall, D. W.; Evanchik, M. A.; Pecoraro, V. L.; Armstrong, W. H.; Britt, R. D. *J. Am. Chem. Soc.* **2000**, *122*, 10926.

(21) Randall, D. W.; Sturgeon, B. E.; Ball, J. A.; Lorigan, G. A.; Chan, M. K.; Klein, M. P.; Armstrong, W. H.; Britt, R. D. *J. Am. Chem. Soc.* **1995**, *117*, 11780.

(22) Tang, X. S.; Sivaraja, M.; Dismukes, G. C. *J. Am. Chem. Soc.* **1993**, *115*, 2382.

(23) Yeagle, G. J.; Gilchrist, M. L.; McCarrick, R. M.; Britt, R. D. *Inorg. Chem.* **2008**, *47*, 1803.

(24) Schweiger, A.; Jeschke, G. *Principles of Pulsed Electron Paramagnetic Resonance*; Oxford University Press: New York, 2001.

(25) Rippka, R.; Deruelles, J.; Waterbury, J. B.; Herdman, M.; Stanier, R. Y. *J. Gen. Microbiol.* **1979**, *111*, 1.

(26) Lakshmi, K. V.; Reifler, M. J.; Chisholm, D. A.; Wang, J. Y.; Diner, B. A.; Brudvig, G. W. *Photosynth. Res.* **2002**, *72*, 175.

(27) Beck, W. F.; Depaula, J. C.; Brudvig, G. W. *Biochemistry* **1985**, *24*, 3035.

(28) Brudvig, G. W. *ACS Symp. Ser.* **1988**, *372*, 221.

(29) Depaula, J. C.; Beck, W. F.; Brudvig, G. W. *J. Am. Chem. Soc.* **1986**, *108*, 4002.

(30) Zheng, M.; Dismukes, G. C. *Inorg. Chem.* **1996**, *35*, 3307.

(31) Garcia-Rubio, I.; Martinez, J. I.; Picorel, R.; Yruela, I. L.; Alonso, P. J. *J. Am. Chem. Soc.* **2003**, *125*, 15846.

(32) Deligiannakis, Y.; Hanley, J.; Rutherford, A. W. *J. Am. Chem. Soc.* **1999**, *121*, 7653.

(33) Deligiannakis, Y.; Rutherford, A. W. *J. Inorg. Biochem.* **2000**, *79*, 339.

(34) Dikanov, S. A.; Xun, L. Y.; Karpiel, A. B.; Tyryshkin, A. M.; Bowman, M. K. *J. Am. Chem. Soc.* **1996**, *118*, 8408.

(35) Astashkin, A. V.; Dikanov, S. A.; Tsvetkov, Y. D. *J. Struct. Chem.* **1984**, *25*, 45.

2D ^{14}N HYSCORE Spectroscopy of the S$_2$ State of Photosystem II

J. Phys. Chem. B, Vol. 114, No. 33, 2010 **10911**

(36) Flanagan, H. L.; Singel, D. J. *J. Chem. Phys.* **1987**, *87*, 5606.

(37) Stoll, S.; Schweiger, A. *J. Magn. Reson.* **2006**, *178*, 42.

(38) Edmonds, D. T. *Phys. Rep., Phys. Lett.* **1977**, *29*, 234.

(39) Ashby, C. I. H.; Cheng, C. P.; Brown, T. L. *J. Am. Chem. Soc.* **1978**, *100*, 6057.

(40) Ashby, C. I. H.; Paton, W. F.; Brown, T. L. *J. Am. Chem. Soc.* **1980**, *102*, 2990.

(41) Tang, X. S.; Diner, B. A.; Larsen, B. S.; Gilchrist, M. L.; Lorigan, G. A.; Britt, R. D. *Proc. Natl. Acad. Sci. U.S.A.* **1994**, *91*, 704.

(42) Blinc, R.; Mali, M.; Osredkar, R.; Seliger, J.; Ehrenber., L. *Chem. Phys. Lett.* **1974**, *28*, 158.

(43) Sproviero, E. M.; McEvoy, J. P.; Gascon, J. A.; Brudvig, G. W.; Batista, V. S. *Photosynth. Res.* **2008**, *97*, 91.

(44) Sproviero, E. M.; Gascon, J. A.; McEvoy, J. P.; Brudvig, G. W.; Batista, V. S. *J. Am. Chem. Soc.* **2008**, *130*, 3428.

(45) Sproviero, E. M.; Shinopoulos, K.; Gascon, J. A.; McEvoy, J. P.; Brudvig, G. W.; Batista, V. S. *Philos. Trans. R. Soc., Ser. B: Biol. Sci.* **2008**, *363*, 1149.

(46) Batista, V.; Sproviero, E.; Gascon, J.; McEvoy, J. P.; Brudvig, G. *Photosyn. Res.* **2007**, *91*, PS42.

(47) Deligiannakis, Y.; Louloudi, M.; Hadjiliadis, N. *Coord. Chem. Rev.* **2000**, *204*, 1.